Membrane Topology of the Colicin E1 Channel Using Genetically Encoded Fluorescence

ARTICLE *in* BIOCHEMISTRY · JUNE 2011

Impact Factor: 3.02 · DOI: 10.1021/bi101934e · Source: PubMed

7 AUTHORS, INCLUDING:

Derek Ho
University of Guelph
3 PUBLICATIONS **16** CITATIONS
SEE PROFILE

Miguel R. Lugo
University of Guelph
21 PUBLICATIONS **233** CITATIONS
SEE PROFILE

Andrei L Lomize
University of Michigan
62 PUBLICATIONS **3,007** CITATIONS
SEE PROFILE

Irina D Pogozheva
University of Michigan
64 PUBLICATIONS **2,014** CITATIONS
SEE PROFILE

BIOCHEMISTRY
including biophysical chemistry & molecular biology

ARTICLE

pubs.acs.org/biochemistry

Membrane Topology of the Colicin E1 Channel Using Genetically Encoded Fluorescence

Derek Ho,[†] Miguel R. Lugo,[†] Andrei L. Lomize,[§] Irina D. Pogozheva,[§] Suneel P. Singh,[‡] Adrian L. Schwan,[‡] and A. Rod Merrill*[,†]

[†]Department of Molecular and Cellular Biology and [‡]Department of Chemistry, University of Guelph, Guelph, ON, Canada N1G 2W1

[§]College of Pharmacy, University of Michigan, Ann Arbor, Michigan 48109-1065, United States

Supporting Information

ABSTRACT: The membrane topology of the colicin E1 channel domain was studied by fluorescence resonance energy transfer (FRET). The FRET involved a genetically encoded fluorescent amino acid (coumarin) as the donor and a selectively labeled cysteine residue tethered with DABMI (4-(dimethylamino)phenylazophenyl-4′-maleimide) as the FRET acceptor. The fluorescent coumarin residue was incorporated into the protein via an orthogonal tRNA/aminoacyl-tRNA synthetase pair that allowed selective incorporation into any site within the colicin channel domain. Each variant harbored a stop (TAG) mutation for coumarin incorporation and a cysteine (TGT) mutation for DABMI attachment. Six interhelical distances within helices 1−6 were determined using FRET analysis for both the soluble and membrane-bound states. The FRET data showed large changes in the interhelical distances among helices 3−6 upon membrane association providing new insight into the membrane-bound structure of the channel domain. In general, the coumarin-DABMI FRET interhelical efficiencies decreased upon membrane binding, building upon the umbrella model for the colicin channel. A tentative model for the closed state of the channel domain was developed based on current and previously published FRET data. The model suggests circular arrangement of helices 1−7 in a clockwise direction from the extracellular side and membrane interfacial association of helices 1, 6, 7, and 10 around the central transmembrane hairpin formed by helices 8 and 9.

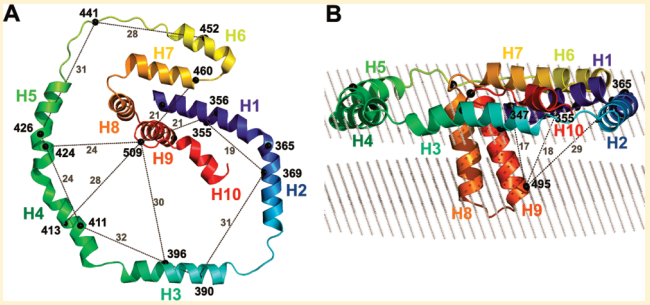

Colicins are antimicrobial proteins produced by *Escherichia coli* that target susceptible bacteria in response to stressful conditions including nutrient depletion, DNA damage, overcrowding, and anaerobiosis.[1] Colicins can be grouped based on their routes of lethal action: (i) the formation of a depolarizing ion channel in the cytoplasmic membrane, (ii) the inhibition of protein and peptidoglycan synthesis, and (iii) the degradation of nucleic acids.[2] Colicin E1 is a member of the ion-channel-forming group of colicins which also includes colicins A, B, Ia, Ib, K, and N.[3,4]

The COOH-terminal channel-forming domain of colicin E1 forms a lethal ion channel which depolarizes the cytoplasmic membrane of target bacterial cells.[5] Prior to channel formation, the channel peptide first binds to the lipid bilayer, followed by protein unfolding and helix elongation.[6−9] Finally, the channel domain adopts an insertion-competent state in which it inserts into membrane to form the prechannel state.[10] The channel then opens in response to a trans-negative membrane potential and facilitates the escape of various ions from the host cells, such as Na^+, K^+, and H^+, leading to host cell death.[11]

The crystal structure of the soluble channel domain (2.5 Å)[12,13] shows 10 α-helices that form an extremely stable, water-soluble globular protein.[14,15] Interestingly, the protein consists of a hydrophobic α-helical hairpin, helices 8 and 9, which acts as the nonpolar core of the protein and becomes transmembrane upon membrane association.[16] These two helices are critical to colicin pore formation by forming a membrane-spanning hairpin that anchors the channel within the bilayer.[17,17−19] The amphipathic α-helices of the channel peptide were shown to surround the hydrophobic core of the channel.[20−23] In the membrane environment, the channel peptide forms a structure previously described as an umbrella in which only the hydrophobic helices 8 and 9 are inserted into the hydrophobic core of the membrane with the amphipathic helices splayed out onto the membrane surface.[24,25] The umbrella model has received strong experimental support from time-resolved FRET studies of colicin E1.[26−28] However, the precise orientation of the helices as well as the details of the lipid and protein contacts are still poorly understood.

It has been shown that the eight amphipathic α-helices on the membrane surface adopt a two-dimensional arrangement with an area of 4200 Å^2, an increase of more than 3-fold of the cross-sectional area of the soluble channel domain.[29] Similarly, FRET data for colicin A revealed that distances generally increase upon

Received: December 3, 2010
Revised: April 28, 2011
Published: April 29, 2011

membrane association.[30−32] Our previous study involved FRET analysis where Cys-505 was labeled with I-AEDANS as acceptor and 11 Trp donor residues were randomly situated throughout the channel domain. These results revealed that higher relative changes in FRET efficiencies were observed the closer the Trp donor was to the N-terminus of the protein.[26]

In support of the umbrella model, the Cramer group adopted a similar approach by using FRET to probe the relative distance of each helix to Cys-509.[29] Although the data could be accounted for by the formation of a quasi-circular arrangement of the eight amphipathic α-helices laying on the membrane surface, a number of other models with various two-dimensional configurations of the helices are also possible. To further test the proposed quasi-circular arrangement model, we used the system developed by Schultz and co-workers to incorporate coumarin into the colicin E1 channel domain to act as an intrinsic FRET donor[33] to DABMI-labeled Cys residues (acceptor). Although labor intensive, this approach can facilitate the construction of a low-resolution 3-D model of the closed channel in the absence of both NMR and X-ray data structural data.

EXPERIMENTAL PROCEDURES

Preparation of Colicin E1 Single-Cys and Single-Stop Codon Variants. All colicin E1 channel domain mutants were prepared by site-directed mutagenesis as previously described.[21] A total of 8 single-Cys and single-stop codon mutants were prepared using the $P190H_6$ construct. Two mutants were used as FRET controls. All plasmids were purified using the High Pure Plasmid isolation kit from Roche Diagnostics (Laval, PQ, Canada), and all mutation sites were confirmed by DNA sequencing (University of Guelph). Each protein variant consists of one single-Cys and one single-stop codon mutation within each adjacent helix from helices 1−6: (F355C/K369stop, helix 1 to 2; K369stop/L390C, helix 2 to 3; L390stop/A411C, helix 3 to 4; A411stop/K426C, helix 4 to 5; K426stop/V441C, helix 5 to 5-loop and V441stop/L452C, helix 5-loop to helix 6).

Synthesis of Coumarin Fluorescent Amino Acid. *Step 1: Synthesis of (2S)-2-benzyloxycarbonylamino-5-oxo-heptanedioic acid 1-benzyl ester 7-ethyl ester.* Carbonyldiimidazole (1.92 g, 11.9 mmol, 1.1 equiv) was added to a solution of *N*-carbobenzyloxy-L-glutamic acid α-benzyl ester (Z-Glu-Obzl, 4.00 g, 10.8 mmol, 1.0 equiv) in dry THF (50 mL) (mixture A) while monoethyl malonate (14.2 g, 108 mmol, 10.0 equiv) was added to magnesium ethoxide (6.16 g, 53.9 mmol, 5.0 equiv) in dry THF (100 mL) (mixture B). Both mixtures were stirred for 4 h at room temperature before mixture A was added slowly to the mixture B, and the stirring continued at room temperature overnight. The solvent was removed *in vacuo*, and the product was dissolved in 20 mL of diethyl ether and 20 mL of 0.5 M HCl. The product was extracted with diethyl ether (3 × 30 mL) and washed with 20 mL of 10% $NaHCO_3$ and 20 mL of brine. The organic layer was treated with anhydrous $MgSO_4$, filtered, and concentrated *in vacuo* to afford a white solid. LC-MS (ESI) calcd for $C_{24}H_{27}NO_7$ ($M + H^+$) 442.18; obsd 442.07. *Step 2: Synthesis of L-(7-hydroxycoumarin-4-yl)ethylglycine.* The product, benzyloxycarbonylamino-5-oxoheptanedioic acid 1-benzyl ester 7-ethyl ester (2.00 g, 4.52 mmol, 1.0 equiv), was added slowly to resorcinol (5.00 g, 45.2 mmol, 10.0 equiv) in methanesulfonic acid (10.9 g, 113 mmol, 25.0 equiv) on ice. The mixture was stirred at room temperature for 4 h. Five volumes of cold ether were added to mixture, which was then cooled at −30 °C for 5 min. The mixture was warmed to room temperature while stirring until a yellow/red solid formed as clumps. The precipitate was washed with cold ether to afford the desired product, which was dissolved in water and used in this study without further purification. LC-MS (ESI) calcd for $C_{13}H_{14}NO_5$ ($M + H^+$) 264.08 Da; obsd 264.14 Da.

Expression and Purification of Coumarin Incorporated Colicin E1 Variants. Both the $P190H_6$ (amp resistance) and pEVOL-CouA (chloramphenicol resistance) plasmids[33] were used to cotransform BL-21 *E. coli* and were plated onto 2xYT media containing both ampicillin and chloramphenicol acetyltransferase selection markers. As a control, BL-21 cells that were transformed with a single plasmid did not grow in the presence of both selection markers. A single colony from the cotransformation was grown overnight at 37 °C (18 h) in 250 mL of 2xYT media supplemented with ampicillin, chloramphenicol, 0.02% arabinose, and 5 mM coumarin amino acid. As a control, another colony was grown under identical conditions, except in the absence of the unnatural amino acid. Successful coumarin incorporation was confirmed by testing for colicin E1 channel domain expression using SDS-PAGE. Variants with proper expression levels were purified as previously described.[22] Protein purity was assessed by SDS-PAGE gel analysis, and protein concentration was determined by absorbance spectroscopy at A_{280}, using the extinction coefficient (ε) of 29 910 M^{-1} cm^{-1} for the WT channel domain.[20] Notably, the extinction coefficient was modified to 39 610 M^{-1} cm^{-1} due to the presence of coumarin within the variants.

Selective Labeling of Single-Cys Variants with DABMI. All 8 single-coumarin, single-Cys variants were selectively labeled with DABMI (4-(dimethylamino)phenylazophenyl-4′-maleimide) to form a DABMI−Cys peptide adduct. The variants were equilibrated in 80 μM DTT in pH 8.1 buffer for 30 min before the DABMI dye was introduced at a 20:1 molar ratio (probe:protein) and incubated for 1 h. The mixture was separated by passing it through a BioRad 10DG 10 mL chromatography column monitoring the eluant by UV absorbance (250−650 nm). The labeling process was the same as previously described.[22] Labeling efficiency was calculated by determining the concentration of protein relative to the concentration of the dye. The following extinction coefficients were used for DABMI−Cys: ε_{460} = 24 800 M^{-1} cm^{-1} and ε_{280} = 8400 M^{-1} cm^{-1},[34] and protein concentration was calculated from the total $Abs_{280\,nm}$ taking into account the contribution from DAMBI−Cys at 280 nm.

Preparation of Large Unilamellar Vesicles (LUVs). LUVs were prepared by an extrusion method from 1,2-dioleoyl-*sn*-glycero-3-phosphocholine and 1,2-dioleoyl-*sn*-glyerco-3-[phospho-*rac*-(1-glycerol)] vesicles at a 60:40 molar ratio (Avanti Polar Lipids, Alabaster, AL) as described earlier.[22] Colicin was bound to liposomes to form a prechannel (closed state) by adding 4 μM colicin channel domain (final concn) in DMG buffer (20 mM dimethyl glutarate, 130 mM NaCl, pH 4.0) to a solution of LUVs (800 μM, final concentration) as described previously.[20,35]

Emission Spectra Measurements. The fluorescence emission of the incorporated coumarin in the absence of acceptor was measured at an excitation wavelength of 365 nm, and emission was scanned between 375 and 650 nm (1 nm steps) and 0.2 s integration time. Excitation and emission band-passes were set at 4 and 6 nm, respectively. Samples were measured in both the presence and absence of LUVs.

Absorbance Spectra Measurements. The absorbance of the DABMI−Cys labeled variants were measured as previously described,[22] except the wavelength was scanned between 250 and 650 nm for the purpose of overlap integral (J) calculations. Absorbances were measured in Helma ultra-microabsorbance cuvettes (light path 10 mm) using a Cary 300 spectrophotometer.

Fluorescence Quantum Yield Measurements. The quantum yields of the protein-incorporated coumarin in the absence of acceptor were measured under identical conditions as described above, except the excitation light was vertically polarized and the emission was measured at the magic angle (54.7°). Quinine sulfate in 0.1 N H_2SO_4 was used as a reference standard, and the quantum yield was calculated as previously described.[22]

Fluorescence Lifetime Measurement. A PTI Laser Strobe model C-72 lifetime fluorimeter was used for the time-resolved fluorescence measurements. Instrument response function (IRF) was measured using a 0.0005% scatter solution. Samples were excited at 365 nm using a pulsed nitrogen dye-laser operated at 10 Hz. Emission was collected at 450 nm with start and end delay set at 58 and 120 ns, respectively. Measurements were carried out with 400 channels, 50 ns, integration time, and 15 shots averaged together at 25 °C.

Fluorescence Lifetime Data Analysis. The data analysis was performed using a 1-to-4 exponential fitting program that involves the deconvolution of the fluorescence decay. Deviations of the best fits were characterized by the reduced χ^2 statistical analysis. In addition, residual graphics, autocorrelation curves, and Durbin−Watson statistics were also used to assess the quality of each fit. The average fluoresence lifetime ($\langle\tau\rangle$) was calculated from the relationship $\langle\tau\rangle = \Sigma\alpha_i\tau_i/\Sigma\alpha_i$ and because $\Sigma\alpha_i = 1$ (normalized pre-exponential values), then $\langle\tau\rangle = \Sigma\alpha_i\tau_i$.

Calculation of FRET Efficiencies and Apparent Distances. FRET efficiency (E) between the donor and acceptor chromophores relates to the inverse sixth power of the distance between the chromophores given by the equation

$$E = \frac{{R_0}^6}{{R_0}^6 + R^6} \tag{1}$$

where E represents the efficiency of energy transfer, R represents the FRET distance separating the two chromophores, and R_0 is the Förster distance, which is the distance when the energy transfer efficiency is 50%. The energy transfer efficiency (E) can be obtained experimentally by either measuring the fluorescence intensity (steady state) or the lifetime (time resolved) of the donor in the presence and absence of the acceptor as described by the equation

$$E = 1 - \frac{F_{DA}}{F_D} = 1 - \frac{\tau_{DA}}{\tau_D} \tag{2}$$

where F_{DA} and F_D represent the fluorescence intensity of the donor in the presence and absence of the acceptor, respectively, and τ_{DA} and τ_D represent the lifetime of the donor in the presence and absence of the acceptor, respectively. The Förster distance (R_0) can be calculated based on the following relationship:

$$R_0 = 9.8 \times 10^3 (J\kappa^2 Q_D \eta^{-4})^{1/6}\ \text{Å} \tag{3}$$

where κ^2 is the orientation factor (assumed to be 2/3), Q_D is the quantum yield of the donor in the absence of acceptor, η is the refractive index of the medium (taken as 1.4),[36] and J is the spectral overlap integral between the donor and acceptor, which is given by the following equation:

$$J = \frac{\int F_D(\lambda)\varepsilon_A(\lambda)\lambda^4\,\delta\lambda}{\int F_D(\lambda)\,\delta\lambda} \tag{4}$$

where F_D is the fluorescence intensity in the presence of the donor only, ε_A is the molar extinction coefficient of the acceptor, and λ is the wavelength. The spectral overlap integral (J) was calculated using a computer program designed by Dr. U. Oehler (University of Guelph) by inputting both the donor (coumarin) emission and the acceptor (DABMI) absorbance spectra.

Modeling the Membrane-Bound Channel Domain. An all-atom model of the membrane-bound domain was generated based on 14 FRET-derived distance constraints obtained in the present work and previously published by Cramer's group.[29] The modeling included two stages. First, all individual α-helices (H1 to H10) and potential membrane-bound α-hairpins (H1−H2, H6−H7, and H8−H9) were taken from the crystal structure of the soluble form (PDB 2i88 file) and spatially arranged in the membrane by minimizing their transfer energy from water to the lipid bilayer using the PPM 2.0 method.[37,38] The method is based on the anisotropic solvent representation of the lipid bilayer described by complex profiles of dielectic constant and hydrogen-bonding parameters along the membrane normal. The calculations were carried out for the native protein and mutants with fluorescent labels (bimane, DABMI, AEDANS, and coumarin) attached to cysteines or genetically incorporated at positions 347, 355, 365, 396, 411, 426, 441, and 509. Side-chain conformers were optimized as previously described.[39] In the second stage, all helices and α-hairpins were brought to the common membrane coordinate frame and manually arranged to fit the set of distance constraints using the molecular modeling module of QUANTA. The helices were considered as rigid bodies with short covalent connections and fixed positions with respect to the membrane plane.

RESULTS

Colicin E1 Variants. Based upon the earlier quasi-circular arrangement model for membrane-bound colicin E1,[29] a number of 2-D configurations of the channel domain on the surface of the bilayer are possible. This is primarily due to the lack of constraints on the model, since there were only five FRET distances (vectors) used in its construction. To reduce the number of possible models, we applied a non-natural amino acid incorporation strategy[33] to genetically encode coumarin fluorescent residues into the channel domain to act as the FRET donors. This method involved extrinsically labeling a Cys residue with DABMI (nonfluorescent acceptor) and then measuring FRET efficiencies between the coumarin (donor fluorophore) and DABMI. The first step involved the preparation of 6 single-stop codon and single-Cys variants to estimate interhelical distances among helices 1 through 6 (Figure 1A). The colicin E1 channel domain sequence and the location of mutation sites within the sequence and the 3-D structure are shown in Figure 1B,C. In this study, the lone Cys residue (Cys-505) was replaced with Ala-505 to avoid the possibility of double Cys labeling. Previous studies confirmed that the C505A mutation does not perturb either the secondary or tertiary structure of the channel domain.[41]

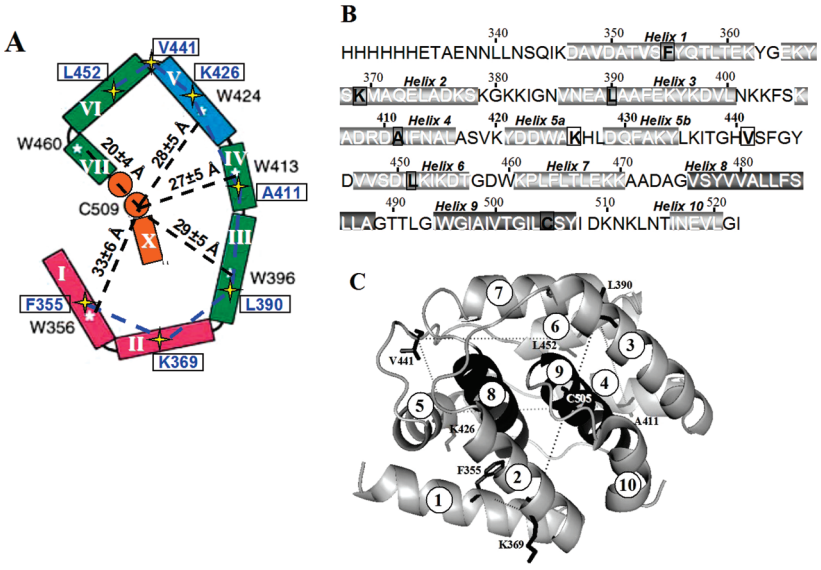

Figure 1. Schematic representation of the colicin E1 channel domain. (A) Quasi-circular arrangement model of the colicin E1 channel domain viewed from the top of the membrane. The 5 FRET distances relative to C509 residue (—) are from a previous report.[29] The 6 interhelical distances connected by stars are the distances measured in this study. (B) The primary sequence and secondary structure of the channel-forming domain of colicin E1 ($P190H_6$). Residues squared in black were subjected to either a stop or Cys codon replacement for the purpose of this study. The natural Cys-505 was replaced with Ala-505. (C) The ribbon topology diagram of the 2.5 Å crystal structure of the P190 peptide (PDB: 2I88). The overall structure consists of 10 α-helices where helices 8 and 9 are the hydrophobic helices (shown in dark) that serve as a membrane-anchoring helical hairpin in the membrane-associated state. The location of the residues subjected to either cysteine or stop codon replacements are shown in sticks and are labeled.

Coumarin Fluorescent Amino Acid Synthesis and Its tRNA/Aminoacyl-tRNA Synthetase Pair System. Coumarin was chosen as the FRET donor due to its relatively high quantum yield, low photobleaching, high stability, and available synthesis.[33] Herein, we report a modified synthetic method with lower cost and greater reproducibility than a previous report[40] but differs from a more recent report.[42] The coumarin derivative (L-(7-hydroxycoumarin-4-yl)ethylglycine) was synthesized by first converting *N*-α-Cbz-L-glutamic acid α-benzyl ester into its side-chain β-ester as shown in Figure 2A (step 1). The second step involved resorcinol condensation with a β-ketoester in the presence of a Brønsted and Lewis acid (methanesulfonic acid) using the von Pechmann reaction pathway to produce the amino acid form.[43−47] Both absorbance and emission spectra of the final product confirmed the amino acid derivative (Figure 2B). NMR (not shown) and mass spectrometry analysis also supported the correct structure and molecular mass of the coumarin fluorescent amino acid (Figure 2C). To enable the incorporation of the coumarin into specific sites within the channel domain, it required an orthogonal tRNA/aminoacyl-tRNA synthetase pair that facilitated the selective introduction of the amino acid into the protein in response to the amber stop codon, TAG. In this study, we utilized the pEVOL-CouA plasmid obtained from the Schultz group.[48] The vector replicates under a p15A origin of replication, it carries the chloramphenicol acetyltransferase (CAT) marker, and it is arabinose inducible. The system features a variant *Methanococcus jannaschii* tyrosyl amber suppressor tRNA ($MjtRNA^{Tyr}_{CUA}$)/tyrosyl-tRNA synthetase (*Mj*TyrRS) pair that was uniquely evolved to recognize the coumarin amino acid in response to the TAG codon. The new pEVOL system was reported to show increased plasmid stability and affords higher yields of variants using both constitutive and inducible promoters to drive the transcription of two copies of the *M. jannaschii* aaRS gene.[48]

Protein Expression and Purification. To optimize colicin expression for coumarin incorporation, a number of parameters were tested as shown in Figure 3. The incubation time did not affect colicin channel domain expression (Figure 3A), and we were able to successfully purify the coumarin-containing variants (K369Cou/L390C example in Figure 3A(v)). Not surprisingly, the percentage of arabinose and the coumarin concentration were the most critical parameters in driving the expression of the channel domain. Induction with 0.02% arabinose in the presence of 5 mM coumarin amino acid were optimal for protein expression as shown in Figure 3A(ii,iii), as found previously.[48] Notably, the BL-21 *E.* coli strain was cotransformed with the various $P190H_6$ mutant plasmids along with the pEVOL-CouA plasmid. Cotransformed colonies were grown in 250 mL of 2xYT media supplemented with ampicillin, chloramphenicol, 0.02% arabinose, and 5 mM coumarin amino acid and incubated at 37 °C for 18 h. Channel domain expression was tested by SDS-PAGE, and it was found that only 5 of the 6 variants showed appreciable expression (Figure 3A(iv)). Since the F355stop/K369C variant showed no expression, its donor/acceptor pair location was swapped to produce the F355C/K369stop variant. Remarkably, the swapping of the donor/acceptor location restored the channel domain expression to an acceptable level (Figure 3A (iv, last lane)). To assess the coumarin incorporation efficiency into the channel domain, the purified K369Cou/L390C variant was subjected to ESI−mass spectrometry analysis. The protein mass was 21 944.2 Da, which nicely correlated with the calculated mass of 21 944.8 Da (Figure 3B). Furthermore, LC-MS/MS analysis confirmed the presence of the coumarin at residue 379 and a Cys residue at position 390 (data not shown). All 8 variants were successfully purified (>95% pure) using immobilized metal-affinity chromatography (IMAC), as previously described.[22]

Folded Integrity of the Coumarin-Tethered Colicin E1 Variants. To assess the structural integrity of the channel domain

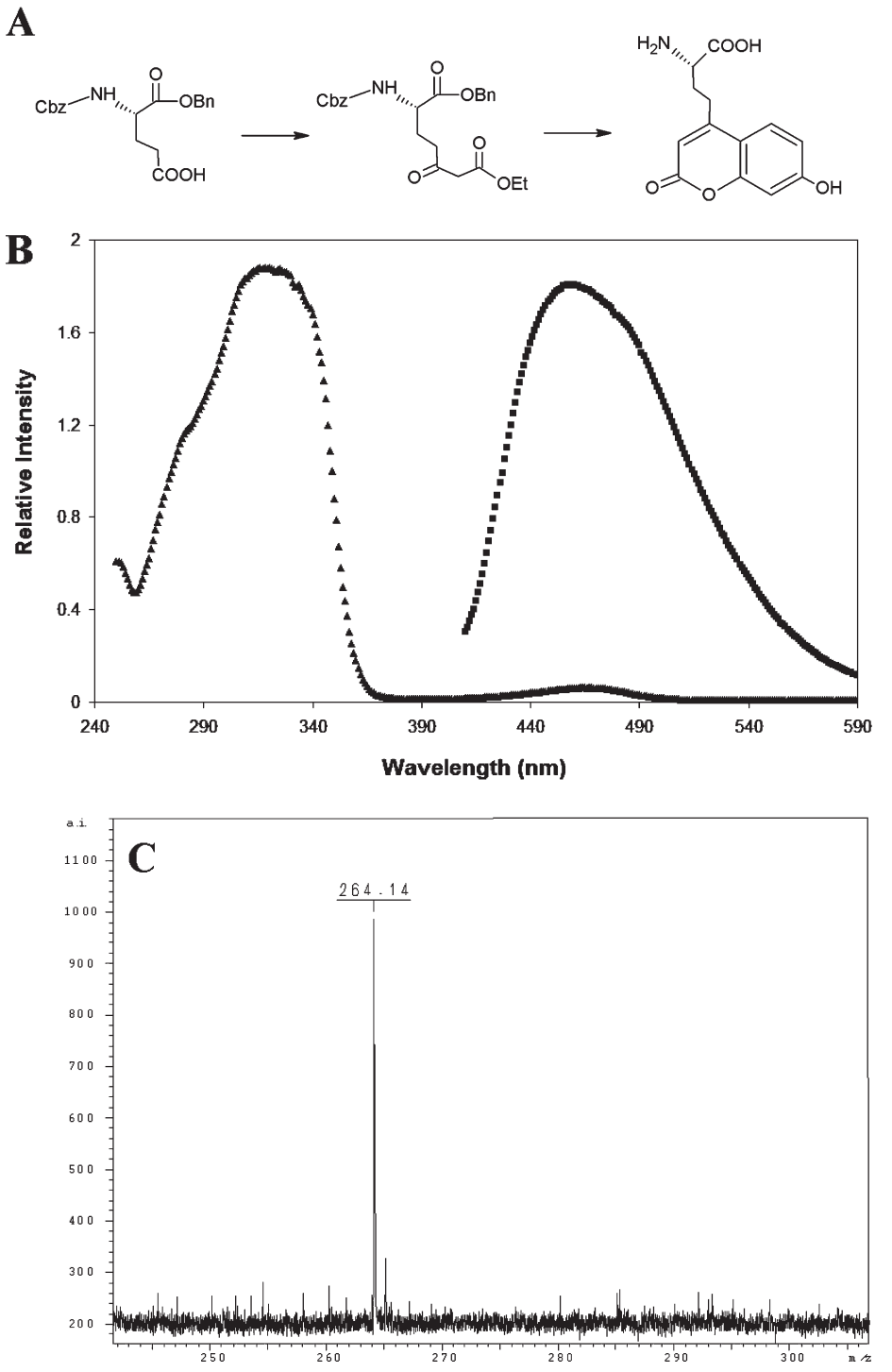

Figure 2. Synthesis of coumarin fluorescent amino acid (L-(7-hydroxycoumarin-4-yl)ethylglycine. (A) Conversion of *N*-α-Cbz-L-glutamic acid α-benzyl ester into the side-chain *β*-keto ester form, followed by reaction with resorcinol in methanesulfonic acid to produce the final coumarin fluorescent amino acid. (B) Absorption (▲) and emission (■) spectra of the purified coumarin fluorescent amino acid. Fluorescence emission intensity was normalized to the absorbance values. (C) Mass spectrometry analysis of the purified coumarin fluorescent amino acid. LC-MS (ESI) calcd for $C_{13}H_{14}NO_5$ ($M + H^+$) 264.08 Da; obsd 264.14 Da.

coumarin variants, Trp fluorescence emission maximum values (Trp $\lambda_{em,max}$) were acquired for the WT and all variants. The WT channel domain gave a Trp $\lambda_{em,max}$ value near 323 nm in good agreement with previous data.[21] The Trp $\lambda_{em,max}$ values of the variants were similar to the WT protein (Table S1). In addition, CD analysis of the variants confirmed that the secondary structure was also similar to the WT protein (Figure S1). Thus, the incorporation of the coumarin residue into the channel domain did not significantly perturb the folded integrity of the variants.

Spectroscopic Measurement of Coumarin and DABMI-Cys Tethered Adducts. To evaluate the chemical structure and properties of the incorporated coumarin, both absorbance and

dx.doi.org/10.1021/bi101934e |*Biochemistry* 2011, 50, 4830–4842

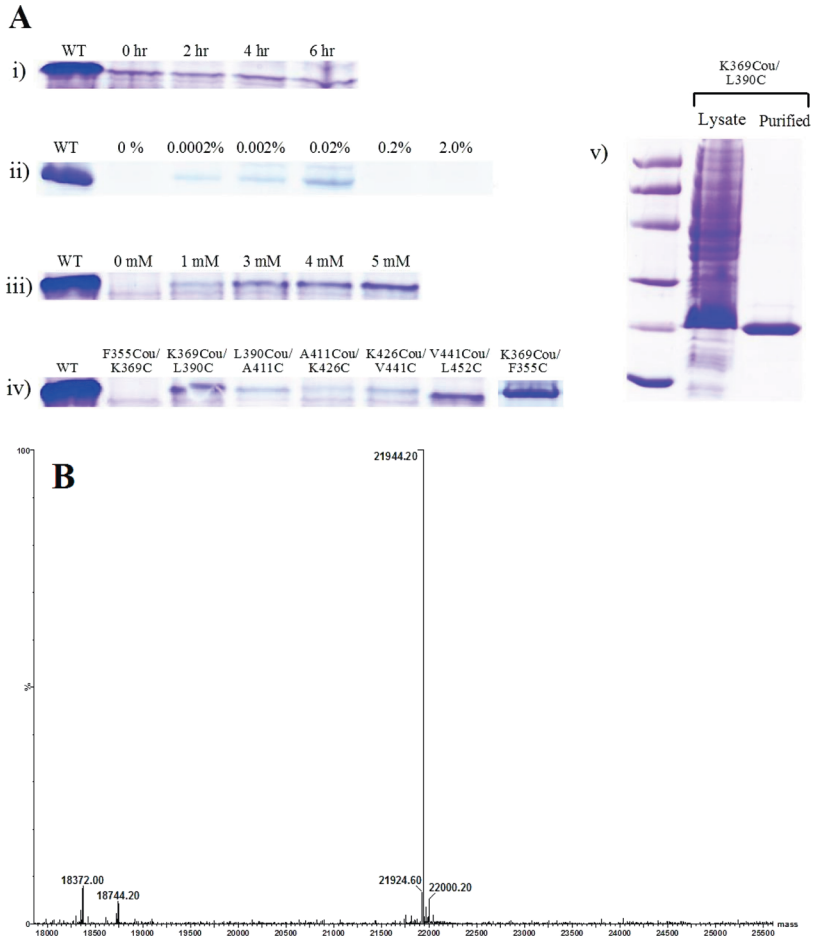

Figure 3. Optimization and expression test of the coumarin-containing colicin E1 channel domain. (A) (i) Expression levels of colicin E1 with 5 mM coumarin amino acid and 0.02% arabinose in the growth medium followed by induction at different time points. (ii) Identical conditions to (i) except arabinose concentration was varied from 0% to 2% and induced at 0 h. (iii) Identical conditions to (i) except the concentration of crude coumarin amino acid was varied from 0 to 5 mM and 0.02% arabinose was added at 0 h. (iv) Expression test of the 6 single-Cys single-stop codon variants in 5 mM coumarin amino acid that was induced with 0.02% arabinose at 0 h. (v) Comparison between purified and nonpurified colicin E1 mutant (K369Cou/L390C). (B) Mass spectrometry analysis of the K369Cou/L390C variant. Mass spectrometry was performed on a Qtof mass spectrometer (Micromass) equipped with a Z-spray source and run in positive ion nanospray mode.

fluorescence emission spectra were collected as shown in Figure 4A. The absorption and fluorescence emission spectra of the K369Cou/L390C variant clearly showed the presence of the coumarin residue within the protein. All 8 variants were subjected to DABMI-Cys labeling, and the representative absorbance spectra for the K369Cou/L390C variant are shown in the presence and absence of covalently tethered DAMBI (Figure 4B). The hallmark peak at 460 nm confirms the successful generation of the DABMI-Cys tethered adducts. Based on the given extinction coefficients for DABMI, $\varepsilon_{460} = 24\,800\ M^{-1}\ cm^{-1}$ and $\varepsilon_{280} = 8400\ M^{-1}\ cm^{-1}$,[45] the labeling efficiencies for all 8 variants ranged between 71% and 108%. The labeling efficiency likely varied due to differences in the solvent accessibility of the target Cys site within the channel domain.

Determination of the Förster Distance (R_0). To determine the distance separating the donor/acceptor chromophores within the channel domain, the initial step involves calculation of the Förster distance (R_0) which is defined as the distance when the energy transfer efficiency is 50%. According to eq 3, this calculation requires knowledge of the quantum yield (Q_F) of the donor (coumarin) in the absence of acceptor as well as the spectral overlap integral (J). The coumarin emission and the DABMI absorption spectra of K369Cou/L390C are shown in Figure 4C. Subtle changes were observed for the coumarin emission spectrum upon membrane association. In general, the intensity of coumarin emission decreased upon the addition of LUVs. In contrast, the coumarin absorbance spectrum remained unchanged upon membrane binding.

To determine the fluorescence quantum yield (Q_F) of the coumarin donor, quinine sulfate was used as a quantum standard. According to Tables 1 and 2, the quantum yield values of coumarin at various sites within the colicin channel domain ranged from 0.52 to 0.81 (an average of 0.67). These values fall within the expected range for coumarin.[33] In general, the quantum yield of the coumarin donors decreased in the lipid-bound state (Table 2). Furthermore, the Förster distance (R_0, Tables 1 and 2) ranged between 13.4 and 26.8 Å for the soluble state and 13.2 and 26.9 Å for the membrane-bound state with an average Förster distance near 22.0 Å for the soluble state and 21.9 Å for the lipid-bound state. Overall, no significant changes were observed between the two states. Importantly, the Förster distance is ideal for this donor/acceptor pair for estimation of the inter-residue distances within the colicin channel domain.

dx.doi.org/10.1021/bi101934e |*Biochemistry* 2011, 50, 4830–4842

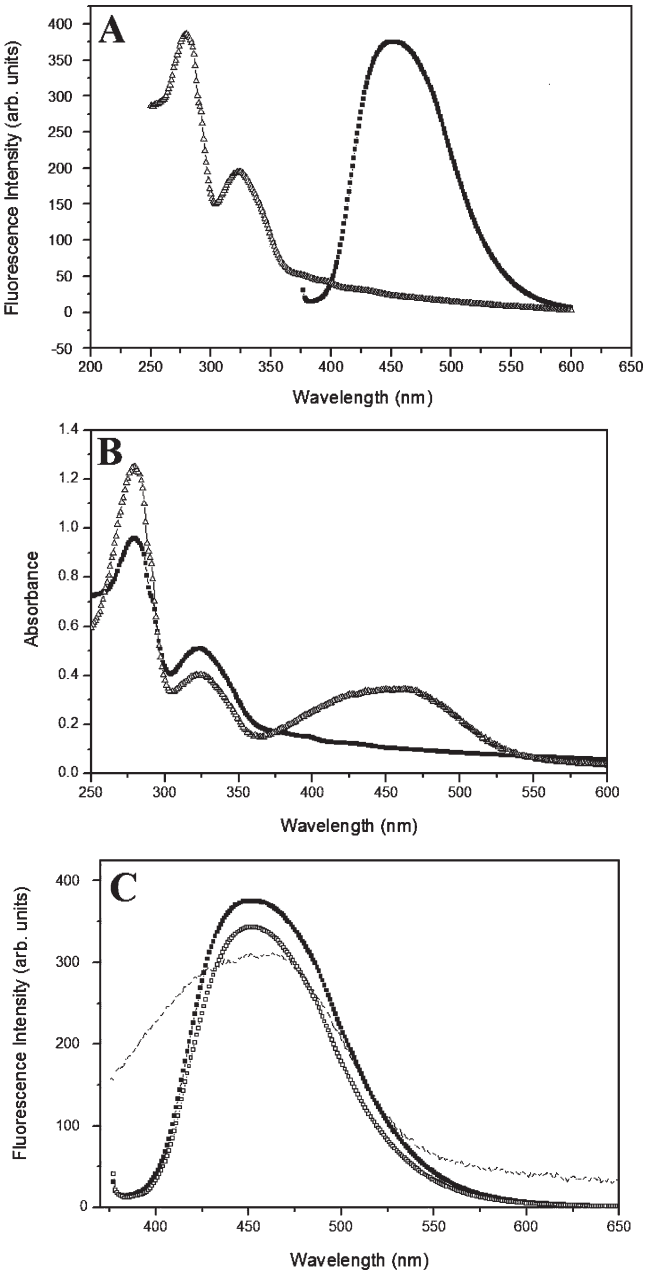

Figure 4. Fluorescence and absorbance spectra of both coumarin and DABMI-Cys tethered adducts within the channel domain in the presence and absence of membrane. (A) Absorption (△) and emission (■) spectra of the coumarin-incorporated K369Cou/L390C variant. Absorbance values were normalized to the fluorescence emission intensity peak for coumarin. (B) Absorption spectra of the purified K369Cou/L390C variant with (△) and without (■) DABMI-Cys labeling. (C) Spectral overlap between the coumarin fluorescence emission spectrum (square symbols) and DABMI absorbance spectrum (—) of the purified K369Cou/L390C variant. Coumarin emission was measured in the presence (□) and absence (■) of membrane to illustrate the changes in the spectral overlap integral. Absorbance units were normalized to the fluorescence emission intensity.

Fluorescence Lifetime Decay Measurements. Accurate FRET measurements require the careful determination of the donor fluorescence lifetime (free coumarin $\tau \cong 5.4$ ns). The coumarin lifetime when tethered to the channel domain showed an average value of 5.98 ns with a range of 5.88−6.12 ns for the soluble state (Tables 1 and 2). In the presence of the DABMI acceptor, the coumarin fluorescence lifetime was reduced depending on the distance between the donor/acceptor pair, as expected (Tables 1 and 2).

FRET Efficiencies within the Channel Domain. The FRET efficiencies between the coumarin donor and DABMI acceptor for colicin channel domain interhelical residues ranged from 59.6% (K369 to F355) to 25.6% (K426 to V441) for the soluble channel domain and from 1.5% (K427 to V441) to 44.8% (K369 to A371) for the membrane-bound protein (Tables 1 and 2; Figure 5A). In general, the FRET efficiencies were smaller in the lipid-bound state compared to the soluble state reflecting the expansion of the channel domain upon binding to the membrane surface.[26] The changes in the FRET efficiencies upon membrane association were all negative in value and ranged from −5.0 to −29.1% (ΔE, Table 2 and Figure 5A). These changes imply that the relative spacing between helices of the channel domain increased upon membrane binding.

FRET-Derived Distances within the Channel Domain. On the basis of eq 1, the FRET distances (R) were calculated as shown in Tables 1 and 2. The inter-residue distances as calculated from the FRET efficiencies ranged from 12.5 Å (K369 to A371) to 29.9 Å (A411 to K426) for the soluble channel domain and from 13.7 Å (K369 to A371) to 40.9 Å (K426 to V441) for the membrane-bound structure (Tables 1 and 2; Figure 5B). All of the distances increased for the measured sites upon membrane binding and ranged from 0.6 Å (K369 to K379) to 17.5 Å (K426 to V441) (ΔR, Table 2).

Comparison of the X-ray Coordinates with FRET Data. To assess both the accuracy and reliability of the data, the FRET distances for the soluble channel domain were plotted against the distances obtained from the X-ray crystal structure,[12,13] as shown in Figure 5C. Although there is a strong correlation in the distance pattern between the two data sets, nonetheless, the FRET distances were generally greater than the X-ray distances. One possible explanation may be the additional length introduced by the covalently linked DABMI acceptor as well as the random orientation angle between the various donor/acceptor pairs. The shorter distances of the crystal structure may be explained because the C_α of each residue was used as the reference point for each measurement.

Closed-State Model of Colicin E1. We have previously demonstrated that this colicin−liposome system used in our present study represents a functionally relevant colicin prechannel state (closed) that upon imposition of a membrane potential forms an active ion channel.[20,35] On the basis of the FRET data in this study, it was found that distances between helices 1 and 2 and between helices 2 and 3 did not change much upon membrane association (Figure 5B). In contrast, the largest changes in helical spacing upon membrane binding occurred between the helix 5 loop and helices 5 and 6. Also, significant increases in distances were observed for helix 3 to 4 and helix 4 to 5 (Figure 5B). To reconcile our new data with the earlier report by Lindeberg and co-workers,[29] we generated a new model of the membrane-bound state using 14 FRET-derived constraints (Table 3). In the first stage of our modeling procedure, spatial positions in the membrane were calculated for individual α-helices and several α-hairpins, whose structures were taken from the water-soluble structure of the protein (Table 4). When associated with the lipid bilayer, most helices are known to remain the same as in the

Table 1. Spectral Parameters and Distances for Fluorescence Energy Transfer between Coumarin Donors and Cys-DABMI Acceptors of the Soluble Colicin E1 Channel Domain

	soluble[a]					
variants	Q_F[b]	R_0[c] (Å)	efficiency[d] (%)	Cou ($\langle\tau\rangle$) − DAB[e] (ns)	Cou ($\langle\tau\rangle$) + DAB[f] (ns)	R[g] (Å)
K369Cou/F355C	0.65 ± 0.06	18.4 ± 0.3	40.7 ± 2.0	5.94 ± 0.08	3.52 ± 0.08	19.6 ± 0.8
K369Cou/L390C	0.67 ± 0.05	26.8 ± 0.3	40.1 ± 0.4	5.94 ± 0.08	3.56 ± 0.04	28.6 ± 0.6
L390Cou/A411C	0.60 ± 0.07	26.6 ± 0.5	38.3 ± 1.9	5.93 ± 0.09	3.66 ± 0.19	28.8 ± 1.8
A411Cou/K426C	0.60 ± 0.05	26.8 ± 0.4	33.9 ± 0.4	6.12 ± 0.03	4.05 ± 0.03	29.9 ± 0.7
K426Cou/V441C	0.75 ± 0.15	19.5 ± 0.7	25.6 ± 4.2	6.01 ± 0.06	4.47 ± 0.24	23.4 ± 2.2
V441Cou/L452C	0.81 ± 0.03	26.4 ± 0.2	37.9 ± 5.9	5.94 ± 0.09	3.68 ± 0.33	28.7 ± 2.3
K369Cou/A371C	0.62 ± 0.02	13.4 ± 0.1	59.6 ± 1.4	6.14 ± 0.10	2.48 ± 0.08	12.5 ± 0.2
K369Cou/K379C	0.67 ± 0.05	18.6 ± 0.2	35.7 ± 1.5	5.88 ± 0.07	3.78 ± 0.08	20.5 ± 0.5

[a] Measurements were with 4 μg/mL protein in DMG buffer at pH 4 (see Experimental Procedures). [b] Quantum yield measurement of the coumarin fluorescent donor in the absence of acceptor (see Experimental Procedures). [c] The Förster distance (R_0) is when the energy transfer efficiency is 50% and was calculated using eq 3 (see Experimental Procedures). [d] The efficiency (E) of energy transfer was calculated according to eq 2 (see Experimental Procedures). [e] The average fluorescence lifetime ($\langle\tau\rangle$) of coumarin (donor) in the absence of DABMI acceptor was calculated from the relationship $\langle\tau\rangle = \Sigma\alpha_i\tau_i/\Sigma\alpha_i$, and because $\Sigma\alpha_i = 1$ (normalized pre-exponential values), then $\langle\tau\rangle = \Sigma\alpha_i\tau_i$. [f] The average fluorescence lifetime ($\langle\tau\rangle$) of coumarin (donor) in the presence of DABMI acceptor. [g] The distance (R) in Å was calculated from the E and R_0 measurements as described in Experimental Procedures.

Table 2. Spectral Parameters and Distances for Fluorescence Energy Transfer between Coumarin Donors and Cys-DABMI Acceptors of the Colicin E1 Channel Domain in the Membrane-Bound State

	LUVs[a]							
variants	Q_F[b]	R_0[c] (Å)	efficiency[d] (%)	Cou ($\langle\tau\rangle$) − DAB[e] (ns)	Cou ($\langle\tau\rangle$) + DAB[f] (ns)	R[g] (Å)	ΔE[h] (%)	ΔR[i] (Å)
K369Cou/F355C	0.63 ± 0.04	18.3 ± 0.2	32.6 ± 0.9	6.15 ± 0.09	4.14 ± 0.08	20.6 ± 0.5	−8.1 ± 0.3	1.0 ± 0.05
K369Cou/L390C	0.62 ± 0.04	26.4 ± 0.3	30.4 ± 0.9	6.94 ± 0.02	4.83 ± 0.07	30.3 ± 0.8	−9.7 ± 0.4	1.7 ± 0.04
L390Cou/A411C	0.52 ± 0.05	26.0 ± 0.4	12.1 ± 2.0	5.96 ± 0.07	5.24 ± 0.08	36.3 ± 3.0	−26.2 ± 1.3	7.5 ± 0.50
A411Cou/K426C	0.62 ± 0.06	26.9 ± 0.4	14.9 ± 2.6	6.08 ± 0.04	5.17 ± 0.13	36.0 ± 2.4	−19.0 ± 0.8	6.1 ± 0.40
K426Cou/V441C	0.70 ± 0.11	20.2 ± 0.6	1.5 ± 0.5	5.93 ± 0.04	5.84 ± 0.04	40.9 ± 4.9	−24.1 ± 2.2	17.5 ± 1.50
V441Cou/L452C	0.66 ± 0.03	25.5 ± 0.2	8.8 ± 3.9	5.93 ± 0.09	5.41 ± 0.11	37.9 ± 3.7	−29.1 ± 3.8	9.2 ± 0.70
K369Cou/A371C	0.57 ± 0.03	13.2 ± 0.1	44.8 ± 1.7	6.03 ± 0.13	3.33 ± 0.08	13.7 ± 0.3	−14.8 ± 0.4	1.2 ± 0.02
K369Cou/K379C	0.64 ± 0.08	18.4 ± 0.4	30.7 ± 2.8	6.28 ± 0.15	4.35 ± 0.16	21.1 ± 1.0	−5.0 ± 0.3	0.6 ± 0.02

[a] Measurements were with 4 μg/mL protein and 800 μM DOPC/DOPG liposomes in DMG buffer (see Experimental Procedures). [b] Quantum yield measurement of the coumarin fluorescent donor in the absence of acceptor (see Experimental Procedures). [c] The Förster distance (R_0) is defined as the distance when the energy transfer efficiency is 50% and was calculated using eq 3 (see Experimental Procedures). [d] The efficiency (E) of energy transfer was calculated according to eq 2 (see Experimental Procedures). [e] The average fluorescence lifetime ($\langle\tau\rangle$) of coumarin (donor) in the absence of DABMI acceptor was calculated from the relationship $\langle\tau\rangle = \Sigma\alpha_i\tau_i/\Sigma\alpha_i$, and because $\Sigma\alpha_i = 1$ (normalized pre-exponential values), then $\langle\tau\rangle = \Sigma\alpha_i\tau_i$. [f] The average fluorescence lifetime ($\langle\tau\rangle$) of coumarin (donor) in the presence of DABMI acceptor. [g] The distance (R) in Å was calculated from the E and R_0 measurements as described in Experimental Procedures. [h] The ΔE (%) was calculated as the $E(\%)_{\text{membrane-bound state}} - \Delta E(\%)_{\text{soluble state}}$. [i] The ΔR (Å) was calculated as the $\Delta R_{\text{membrane-bound state}} - \Delta R_{\text{soluble state}}$.

crystal structure,[20−22,41] while H3 may be elongate by a few residues.[20]

According to the calculations, individual amphipathic helices (from H1 to H7, and H10) are located at the membrane surface with nonpolar residues inserted in the hydrocarbon core below the boundary formed by carbonyl groups of phospholipids (Table 4). The surface helices have tilt angles of 80°−90° with respect to the membrane normal. H1 appears to be the most tilted helix with the N-terminus inserted at the depth of ∼8 Å, in agreement with fluorescence spectroscopy studies.[21] Transfer energies of surface helices are −3.5 to −10.5 Kcal/mol. H2 and H10 demonstrated the weakest membrane binding (transfer energies of −4.5 and −3.5 kcal/mol, respectively), while H1 showed the largest binding energy for the individual surface-located helix (ΔG_{transf} = −10.5 kcal/mol). In contrast, the more hydrophobic H8 and H9 helices likely adopt a transmembrane orientation (transfer energies of −12.5 and −14 kcal/mol and tilt angles of 27° and 54°, respectively). The incorporation of fluorescent probes into the interfacial sites only slightly affected the arrangement of helices in membrane (the largest effect was seen for H1 labeled at F355C).

We also considered the possibility of the formation of stable membrane-bound α-hairpins by H1−H2, H6−H7, and H8−H9 pairs found in the crystal structure of the soluble channel domain. Significant binding energies of H6−H7 and H8−H9 pairs (−9.8 and −15.9 kcal/mol, respectively) indicate that these helices could interact with membrane as α-hairpins. In contrast, energy transfer between the H1−H2 pair was small and less than for individual H1 and H2 helices, indicating that H1 and H2 may dissociate and rearrange in the membrane-bound state, unlike H6−H7 and H8−H9 pairs.

dx.doi.org/10.1021/bi101934e |*Biochemistry* 2011, 50, 4830–4842

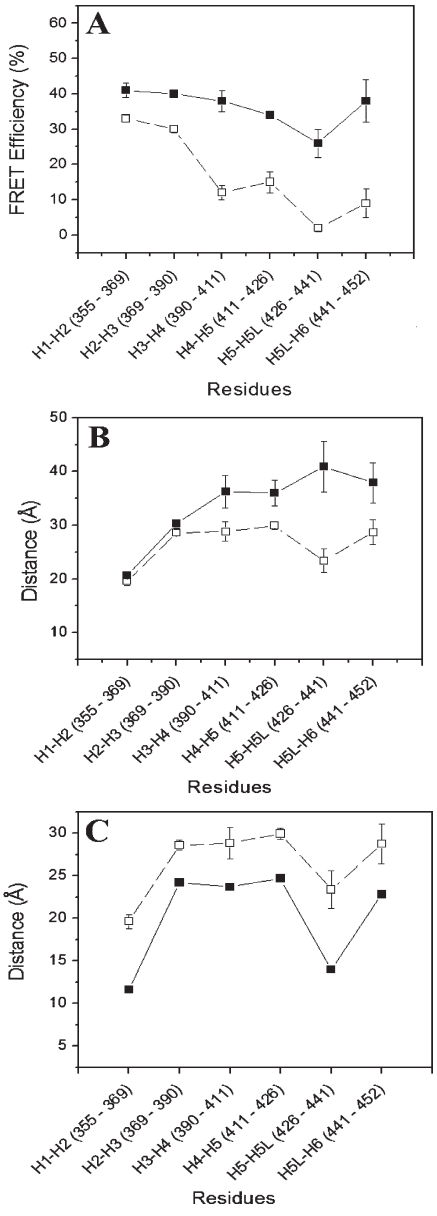

Figure 5. Apparent distances and energy transfer efficiencies between the various donor (coumarin) and acceptor (DABMI) pairs within colicin E1. (A) The energy transfer efficiencies for the various donor and acceptor pairs were determined by lifetime analysis of the coumarin donors in the presence and absence of the DABMI acceptor. Changes of the energy transfer efficiency were compared between the soluble (■) and membrane-bound states (□). The mean score for soluble state ($M = 0.36$ SD = 0.003, $N = 6$) was significantly larger than the scores for membrane-bound state ($M = 0.17$, SD = 0.015, $N = 6$) using the two-sample t test for unequal variances, $t(5) = 5.47$, $p \leq 0.003$. (B) Apparent distances between the various donor and acceptor pairs were measured by FRET in both the soluble (□) and membrane-bound states (■). The mean score for the soluble state ($M = 26.52$ SD = 8.35, $N = 6$) was significantly lower than the scores for membrane-bound state ($M = 33.66$, SD = 26.32, $N = 6$) using the two-sample t test for unequal variances, $t(5) = 2.91$, $p \leq 0.03$. The numbers in parentheses correspond to the donor and acceptor sites (residue numbers within the colicin channel domain) for the FRET efficiency measurements. (C) Comparison between the soluble FRET distances (□) and the estimated distances based on the X-ray crystal structure (PDB: 2i88) of the soluble state (■). The α-carbon atom was used as a reference point for all crystal structure distance measurements.

Membrane-penetration depth ($D \sim 19$ Å) and tilt angle ($\tau \sim 14°$) of the α-hairpin H8−H9 suggest that it likely traverses the membrane, leading to the local membrane thinning. The comparison of the binding energy of the H8−H9 α-hairpin in transmembrane (−15.9 kcal/mol) and surface (−8.8 kcal/mol) orientations further justifies its transmembrane arrangement. The parameters of α-hairpin H6−H7 ($D \sim 4$ Å, $\tau \sim 88°$) indicate its surface location. Hence, our results suggest the existence of two stable membrane-bound α-hairpins, H6−H7 and H8−H9, which are stabilized by short turns and the classic "knobs into holes" packing of interacting helices with an interhelical angle of ∼−160°, as observed in the crystal structure of the water-soluble channel domain.

In the next modeling stage, all helices and α-hairpins H6−H7 and H8−H9 were brought to the common membrane coordinate system and arranged to fit the set of distance constraints (Table 3). The modeling is simplified by the presence of short connections between almost all helices. Hence, a distance between residues from adjacent helices translates to an interhelical angle, which defines the mutual arrangement of two helices at membrane surface. The close distances (∼20 Å) between residues from H9 (W495) and H1 (347, 355), H7 (W460) and between H1 (355) and H2 (369) define the proximity of surface helices H1, H7 to H9 and circular helix arrangement with clockwise direction as viewed from the extracellular surface (Figure 6). This model also suggests aggregation of predicted α-hairpin H6−H7 and helices H1, H10 around the transmembrane α-hairpin H8−H9.

The proposed model satisfies most of the FRET-derived distances, except those with H5a (residues 424 and 426). However, this region of H5 is highly distorted in the crystal structure and might be unfolded upon membrane binding, which would increase the distances involving residues 424 and 426. Another discrepancy was observed for the 509−356 distances (Table 4). The smaller distance between Cα-atoms in the model (by 12 Å) may be observed because fluorescent probes attached to these residues are oriented in the opposite directions. A similar situation with large FRET distances was experimentally observed for labels located in H2 at proximal residues 369 and 371 oriented in the opposite directions (distance ∼13 Å, Table 1).

■ DISCUSSION

NMR has contributed to our understanding of the membrane-bound structure of colicin;[16,49,50] unfortunately to date, neither NMR nor X-ray crystallography methods have been able to provide a membrane-bound structure of colicin E1. FRET appears as the only viable alternative to provide sufficient data for a low-resolution 3-D model of the membrane-bound protein. Although it is a tedious and labor-intensive process that would require hundreds of variants, it can be achieved based upon the results of the present study. According to a previous model, the channel domain forms an umbrella-like shape with helices 8 and 9 forming a transmembrane helical anchor with its amphipathic helices laying parallel on the membrane surface in a quasi-circular arrangement surrounding helices 8 and 9.[29]

Herein, we used a new FRET-based approach involving the engineering of the non-natural fluorescent amino acid, coumarin, into the channel domain as the fluorescence donor. Consequently, in combination with an extrinsically labeled cysteine as the fluorescent acceptor, both inter- and intrahelical distances can more readily be obtained. In this study, we report the success

Table 3. Comparison of FRET-Derived Distance Constraints (R) and Cα−Cα Distances from the Calculated Model of the Membrane-Bound Closed State of the Colicin E1 Channel Domain

variants	R, Å (FRET)	Cα−Cα, Å (model)	helix−helix
D347C-bimane/W495	20.5	17.4	H1/H9
F355C-bimane/W495	23	17.5	H1/H9
E365C-bimane/W495	31.8	29.0	H2/H9
F355C-DABMI/K369Cou	20.6	19.1	H1/H2
K369Cou/L390C-DABMI	30.3	30.7	H2/H3
L390Cou/A411C-DABMI	36.3	32.0	H3/H4
A411Cou/K426C-DABMI	36.0	24.3	H4/H5
K426Cou/A441C-DABMI	40.9	31.3	H5/loop(5−6)
A441Cou/L452C-DABMI	37.9	27.8	loop(5−6)/H6
D509C-AEDANS/Y356W	33	21.3	loop(9−10)/H1
D509C-AEDANS/Y396W	29	30.2	loop(9−10)/H3
D509C-AEDANS/F413W	27	27.7	loop(9−10)/H4
D509C-AEDANS/W424	28	23.7	loop(9−10)/H5
D509C-AEDANS/W460	21	20.9	loop(9−10)/H6

Table 4. Membrane Binding Energies (ΔG_{transf}), Membrane Penetration Depths (D), and Tilt Angles Relative to the Membrane Normal (τ) of Individual α-Helices and α-Hairpins of Colicin E1 Channel Domain Calculated Using PPM 2.0

helix	D,[a] Å	τ, deg	ΔG_{transf}, kcal/mol
H1	7.7 ± 1.5[a]	78 ± 39	−10.5
H2	4.6 ± 1.7[a]	84 ± 15	−4.5
α hairpin(H1−H2)	3.8 ± 2.2[a]	87 ± 6	−3.4
H3	4.2 ± 1.0[a]	88 ± 21	−7.1
H4	4.6 ± 1.7[a]	81 ± 13	−6.6
H5	4.8 ± 0.6[a]	80 ± 10	−8.4
H6	2.8 ± 3.8[a]	90 ± 3	−7.4
H7	4.7 ± 1.2[a]	85 ± 12	−6.1
α hairpin(H6−H7)	3.7 ± 0.4[a]	88 ± 6	−9.8
H8	18.8 ± 1.4[b]	27 ± 33	−12.5
H9	19.0 ± 2.4[b]	54 ± 27	−14.0
α hairpin(H8−H9)	18.8 ± 0.5[b]	14 ± 21	−15.9
H10	2.0 ± 1.0[a]	82 ± 16	−3.5

[a] D = depth of membrane insertion[a] (for surface helices) or hydrophobic thickness[b] (for transmembrane helices). The uncertainty of parameters (± values) was estimated as maximal amplitude of their fluctuations within ±1 kcal/mol around global minimum of transfer energy.[39]

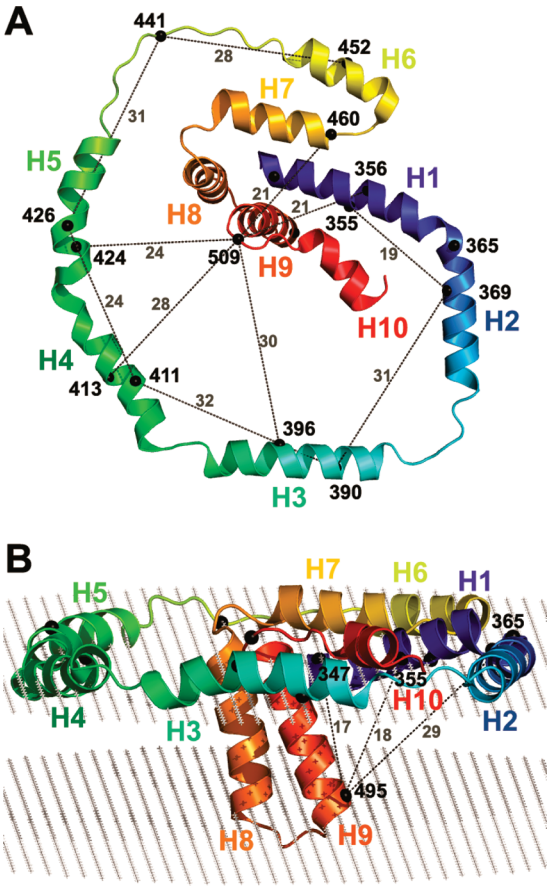

Figure 6. Membrane-bound closed-state model of the colicin E1 channel domain, top (A) and side (B) views. Helices are shown by cartoon, colored rainbow; hydrocarbon core boundaries corresponding to the location of lipid carbonyl groups are indicated by gray dots. Cα atoms of labeled residues used in FRET experiments are shown by numbered black dots. Distances between labeled residues in the model are indicated by gray numbers near the black dashes.

of applying this technique to generate coumarin-derived colicin E1 variants. Mass spectrometry analysis confirmed the success of both the synthesis of coumarin fluorescent amino acid as well as its successful incorporation into the colicin E1 channel domain.

We propose that the generation of an intrinsic coumarin fluorescence donor greatly reduces the FRET-measured error associated with the technique. This is largely due to the elimination of nonspecific labeling when two covalent attachment sites serve as the donor/acceptor pairs. We chose DABMI as the FRET acceptor due to its small size, high quantum yield, its large spectral overlap integral with coumarin (donor) emission, and that it has no intrinsic fluorescence. The DABMI compound exhibits a well-defined covalent bonding angle with a Cys residue, and it is generally free to rotate when tethered to a protein surface. Consequently, it may help minimize the error associated with the orientation factor (κ^2).[51]

dx.doi.org/10.1021/bi101934e |*Biochemistry* 2011, 50, 4830–4842

It was fortunate that most variants in this study showed reasonably good expression. However, as shown in Figure 3A, no colicin expression was observed for F355Cou/K369C variant, but upon reversal of the donor/acceptor pair location, protein expression was recovered. Herein, it should be noted that the coumarin incorporation system[33] has a limitation in the sensitivity of each fluorescence residue to the site of incorporation within the protein, which impacts the incorporation efficiency. In fact, we were unable to obtain reliable FRET data for a distance estimate between helices 6 and 7 because of the difficulty in finding a suitable incorporation site for the coumarin within helix 7. Unfortunately, no single rule can be applied to govern the incorporation efficiency for each residue. However, previous experiments suggested that expressing variants in richer media with higher fluorescent amino acid concentrations does improve incorporation efficiency.[48]

In this study, a high correlation was found between the FRET distances for the soluble channel domain and the distances estimated from the X-ray crystal structure. Although minor variations were present, most of the deviation could be explained by the size and flexibility of the donor and acceptor chromophores. In general, the FRET data in this study are in good agreement with previously reported FRET data.[26,29] Our data further extend those of previous reports and clearly show that the distances separating helices 1−3 within the colicin channel domain remain relatively unchanged upon membrane binding, whereas the distances separating helices 3−6 significantly increase for the lipid-bound state. In particular, the helix 5−6 loop region was shown to be highly mobile, and the FRET data suggest that it opens up on the membrane surface upon channel domain insertion into the bilayer. The fact that both control variants, K369Cou/A371C and K369Cou/K379C, showed little or no distance changes between the soluble and membrane-bound states suggests that helix 2 within the channel domain remains unchanged in both the soluble and lipid-bound states, which corroborates our previous findings.[21] Spacing changes among helices 3−6 suggest that major structural rearrangements occur in this region of the channel domain upon membrane association. Previously, solid-state NMR experiments by Hong and colleagues[52] demonstrated that the membrane-bound prechannel state of colicin Ia is considerably more mobile than the water-soluble structure, and this observation correlates nicely with the need for enhanced protein mobility to form the open channel. Our FRET measurements herein represent only an average measurement of this dynamic structure, and there is likely more than one substate/conformation for the prechannel structure. Our goal is to study the dynamic aspects of this structure and to map the relative mobility of the prechannel state using time-resolved fluorescence anisotropy measurements. However, despite the increased mobility of the channel domain upon membrane binding, we have noted that our FRET data distance distribution function is relatively narrow as are the distributions of the lifetime decay curves (relatively sharp) for the donor lifetimes. This indicates that there is still real, constrained tertiary structure in the colicin membrane-bound prechannel state and that it has not lost its core structure. Our previous results using hydrophobic periodicity analysis[20−22,41] clearly showed that the secondary structure (helical content) of the prechannel state increases among helices 1−6 upon membrane binding. Based on our FRET measurements, both control variants, K369Cou/A371C and K369Cou/K379C, showed little or no distance changes between the soluble and membrane-bound states, suggesting that helix 2 within the channel domain remains unchanged in both the soluble and lipid-bound states, which corroborates our previous findings.[21] Notably, spacing changes among helices 3−6 suggest that major structural rearrangements occur in this region of the channel domain upon membrane association, which support the previous NMR findings on the enhanced mobility of the prechannel structure[52] and are also supported by computational studies.[53]

Although a wide array of two-dimensional configurations are possible for the closed-state of the channel domain on the membrane surface, the FRET-derived data in this study help eliminate a number of possibilities, including the previously published quasi-circular model of Cramer.[29] In summary, our proposed model (Figure 6) also demonstrates the circular arrangement of the helices in the membrane-bound state. New features of the current model are (a) the clockwise direction of helix arrangement as viewed from the extracellular surface, (b) the presence of surface H6−H7 and transmembrane H8−H9 α-hairpins, and (c) the formation of a cluster formed by helices H1, H2, H7−H6, and H10 that pack around the transmembrane hairpin, H8−H9, which acts as a nucleation center. Importantly, our working model represents an important step forward toward our goal of determining the membrane-bound structure of the closed state of colicin E1. This model accounts for the previous data[29] as well as our new FRET data and helps explain why FRET donors near the amino terminus show larger changes in energy transfer efficiency as compared with the central region of the channel domain.[26] To further refine this model, our goal is to continue this approach to provide a greater number of constraints and to improve its overall resolution. In the future, we also plan to use a similar FRET technique to study the topology of the open channel state in a helix-by-helix fashion. However, this would require the presence of a membrane potential using supported planar bilayers on gold electrodes that are still currently under development.

■ ASSOCIATED CONTENT

Supporting Information. A method for the synthesis of (2*S*)-2-benzyloxycarbonylamino-5-oxoheptanedioic acid 1-benzyl ester 7-ethyl ester, Table S1 (fluorescence emission maxima for the coumarin-tethered colicin mutants), and Figure S1 (CD spectra of WT and mutant colicin proteins). This material is available free of charge via the Internet at http://pubs.acs.org.

■ AUTHOR INFORMATION

Corresponding Author

*Tel: (519) 824-4120 x53806. Fax: (519) 837-1802. E-mail: rmerrill@uoguelph.ca.

Funding Sources

This work was supported by grants from the Natural Sciences and Engineering Research Council of Canada (to A.L.S. and A.R.M.) and from the National Science Foundation, Division of Biological Infrastructure (Grant 0849713) (to A.L.L.).

■ ACKNOWLEDGMENT

We thank Dr. Peter Schultz for kindly providing the pEVOL-CouA plasmid. We also thank both Gerry Prentice and Dawn White for their technical assistance throughout this study.

■ ABBREVIATIONS

P190H$_6$, colicin E1 190 residue channel domain with an N-terminal 6 histidine tag; DMG, dimethylglutaric acid; DABMI (4-(dimethylamino)phenylazophenyl-4′-maleimide) DTT, dithiothreitol; DOPC, 1,2-dioleoyl-*sn*-glycero-3-phosphocholine; DOPG, 1,2-dioleoyl-*sn*-glycero-3-[phosphorac-(1-glycerol)]; FRET, fluorescence resonance energy transfer; LUVs, large unilamellar vesicles; PBS, phosphate-buffered saline; $\lambda_{em\,max}$, fluorescence wavelength emission maximum; WT, wild-type.

■ REFERENCES

(1) Pugsley, A. P. (1984) The ins and outs of colicins. Part II. Lethal action, immunity and ecological implications. *Microbiol. Sci. 1*, 203–205.

(2) Cascales, E., Buchanan, S. K., Duche, D., Kleanthous, C., Lloubes, R., Postle, K., Riley, M., Slatin, S., and Cavard, D. (2007) Colicin biology. *Microbiol. Mol. Biol. Rev. 71*, 158–229.

(3) Filloux, A., Voulhoux, R., Ize, B., Gerard, F., Ball, G., and Wu, L. F. (2002) Use of colicin-based genetic tools for studying bacterial protein transport. *Biochimie 84*, 489–497.

(4) Zakharov, S. D., Kotova, E. A., Antonenko, Y. N., and Cramer, W. A. (2004) On the role of lipid in colicin pore formation. *Biochim. Biophys. Acta 1666*, 239–249.

(5) Cramer, W. A., Heymann, J. B., Schendel, S. L., Deriy, B. N., Cohen, F. S., Elkins, P. A., and Stauffacher, C. V. (1995) Structure-function of the channel-forming colicins. *Annu. Rev. Biophys. Biomol. Struct. 24*, 611–641.

(6) Zakharov, S. D., Lindeberg, M., and Cramer, W. A. (1999) Kinetic description of structural changes linked to membrane import of the colicin E1 channel protein. *Biochemistry 38*, 11325–11332.

(7) Shin, Y. K., Levinthal, C., Levinthal, F., and Hubbell, W. L. (1993) Colicin E1 binding to membranes: time-resolved studies of spin-labeled mutants. *Science 259*, 960–963.

(8) Cramer, W. A., Zhang, Y. L., Schendel, S., Merrill, A. R., Song, H. Y., Stauffacher, C. V., and Cohen, F. S. (1992) Dynamic properties of the colicin E1 ion channel. *FEMS Microbiol. Immunol. 5*, 71–81.

(9) Elkins, P., Bunker, A., Cramer, W. A., and Stauffacher, C. V. (1997) A mechanism for toxin insertion into membranes is suggested by the crystal structure of the channel-forming domain of colicin E1. *Structure 5*, 443–458.

(10) Tian, C., Tetreault, E., Huang, C. K., and Dahms, T. E. (2006) Electrostatic interactions of colicin E1 with the surface of Escherichia coli total lipid. *Biochim. Biophys. Acta 1758*, 693–701.

(11) Gouaux, E. (1997) The long and short of colicin action: the molecular basis for the biological activity of channel-forming colicins. *Structure 5*, 313–317.

(12) Elkins, P. A., Song, H. Y., Cramer, W. A., and Stauffacher, C. V. (1994) Crystallization and characterization of colicin E1 channel-forming polypeptides. *Proteins 19*, 150–157.

(13) Parker, M. W., Postma, J. P., Pattus, F., Tucker, A. D., and Tsernoglou, D. (1992) Refined structure of the pore-forming domain of colicin A at 2.4 A resolution. *J. Mol. Biol. 224*, 639–657.

(14) Schendel, S. L., and Cramer, W. A. (1994) On the nature of the unfolded intermediate in the in vitro transition of the colicin E1 channel domain from the aqueous to the membrane phase. *Protein Sci. 3*, 2272–2279.

(15) Griko, Y. V., Zakharov, S. D., and Cramer, W. A. (2000) Structural stability and domain organization of colicin E1. *J. Mol. Biol. 302*, 941–953.

(16) Kim, Y., Valentine, K., Opella, S. J., Schendel, S. L., and Cramer, W. A. (1998) Solid-state NMR studies of the membrane-bound closed state of the colicin E1 channel domain in lipid bilayers. *Protein Sci. 7*, 342–348.

(17) Zakharov, S. D., and Cramer, W. A. (2002) Colicin crystal structures: pathways and mechanisms for colicin insertion into membranes. *Biochim. Biophys. Acta 1565*, 333–346.

(18) Lesieur, C., Vecsey-Semjen, B., Abrami, L., Fivaz, M., and Gisou van der, G. F. (1997) Membrane insertion: The strategies of toxins (review). *Mol. Membr. Biol. 14*, 45–64.

(19) Song, H. Y., and Cramer, W. A. (1991) Membrane topography of ColE1 gene products: the immunity protein. *J. Bacteriol. 173*, 2935–2943.

(20) Wei, Z., White, D., Wang, J., Musse, A. A., and Merrill, A. R. (2007) Tilted, extended, and lying in wait: the membrane-bound topology of residues lys-381-ser-405 of the colicin e1 channel domain. *Biochemistry 46*, 6074–6085.

(21) White, D., Musse, A. A., Wang, J., London, E., and Merrill, A. R. (2006) Toward elucidating the membrane topology of helix two of the colicin e1 channel domain. *J. Biol. Chem. 281*, 32375–32384.

(22) Musse, A. A., Wang, J., Deleon, G. P., Prentice, G. A., London, E., and Merrill, A. R. (2006) Scanning the membrane-bound conformation of helix 1 in the colicin E1 channel domain by site-directed fluorescence labeling. *J. Biol. Chem. 281*, 885–895.

(23) Salwinski, L., and Hubbell, W. L. (1999) Structure in the channel forming domain of colicin E1 bound to membranes: the 402−424 sequence. *Protein Sci. 8*, 562–572.

(24) Lins, L., El, K. K., Charloteaux, B., Flore, C., Stroobant, V., Thomas, A., Dufrene, Y., and Brasseur, R. (2007) Lipid-destabilizing properties of the hydrophobic helices H8 and H9 from colicin E1. *Mol. Membr. Biol. 24*, 419–430.

(25) Tory, M. C., and Merrill, A. R. (1999) Adventures in membrane protein topology. A study of the membrane-bound state of colicin E1. *J. Biol. Chem. 274*, 24539–24549.

(26) Steer, B. A., and Merrill, A. R. (1994) The colicin E1 insertion-competent state: detection of structural changes using fluorescence resonance energy transfer. *Biochemistry 33*, 1108–1115.

(27) Zakharov, S. D., Lindeberg, M., Griko, Y., Salamon, Z., Tollin, G., Prendergast, F. G., and Cramer, W. A. (1998) Membrane-bound state of the colicin E1 channel domain as an extended two-dimensional helical array. *Proc. Natl. Acad. Sci. U.S.A. 95*, 4282–4287.

(28) Palmer, L. R., and Merrill, A. R. (1994) Mapping the membrane topology of the closed state of the colicin E1 channel. *J. Biol. Chem. 269*, 4187–4193.

(29) Lindeberg, M., Zakharov, S. D., and Cramer, W. A. (2000) Unfolding pathway of the colicin E1 channel protein on a membrane surface. *J. Mol. Biol. 295*, 679–692.

(30) Lakey, J. H., and Slatin, S. L. (2001) Pore-forming colicins and their relatives. *Curr. Top. Microbiol. Immunol. 257*, 131–161.

(31) Duche, D., Izard, J., Gonzalez-Manas, J. M., Parker, M. W., Crest, M., Chartier, M., and Baty, D. (1996) Membrane topology of the colicin A pore-forming domain analyzed by disulfide bond engineering. *J. Biol. Chem. 271*, 15401–15406.

(32) Duche, D., Baty, D., Chartier, M., and Letellier, L. (1994) Unfolding of colicin A during its translocation through the Escherichia coli envelope as demonstrated by disulfide bond engineering. *J. Biol. Chem. 269*, 24820–24825.

(33) Wang, L., Xie, J., and Schultz, P. G. (2006) Expanding the genetic code. *Annu. Rev. Biophys. Biomol. Struct. 35*, 225–249.

(34) Luo, Y., Leszyk, J., Li, B., Gergely, J., and Tao, T. (2000) Proximity relationships between residue 6 of troponin I and residues in troponin C: further evidence for extended conformation of troponin C in the troponin complex. *Biochemistry 39*, 15306–15315.

(35) Musse, A. A., and Merrill, A. R. (2003) The molecular basis for the pH-activation mechanism in the channel-forming bacterial colicin E1. *J. Biol. Chem. 278*, 24491–24499.

(36) Piston, D. W., and Kremers, G. J. (2007) Fluorescent protein FRET: the good, the bad and the ugly. *Trends Biochem. Sci. 32*, 407–414.

(37) Lomize, A. L., Pogozheva, I. D., and Mosberg, H. I. (2011) Anisotropic Solvent Model of the Lipid Bilayer. 1. Parameterization of Long-Range Electrostatics and First Solvation Shell Effects. *J. Chem. Inf. Model. 51*, 918–929.

(38) Lomize, A. L., Pogozheva, I. D., and Mosberg, H. I. (2011) Anisotropic Solvent Model of the Lipid Bilayer. 2. Energetics of Insertion of Small Molecules, Peptides, and Proteins in Membranes. *J. Chem. Inf. Model. 51*, 930–946.

(39) Lomize, A. L., Pogozheva, I. D., Lomize, M. A., and Mosberg, H. I. (2006) Positioning of proteins in membranes: a computational approach. *Protein Sci. 15*, 1318–1333.

(40) Wang, J., Xie, J., and Schultz, P. G. (2006) A genetically encoded fluorescent amino acid. *J. Am. Chem. Soc 128*, 8738–8739.

(41) Ho, D., and Merrill, A. R. (2009) Evidence for the amphipathic nature and tilted topology of helices 4 and 5 in the closed state of the colicin E1 channel. *Biochemistry 48*, 1369–1380.

(42) Braun, M., and Dittrich, T. (2010) Synthesis of the fluorescent amino acid rac-(7-hydroxycoumarin-4-yl)ethylglycine. *Beilstein J. Org. Chem. 6*, ii:69.

(43) Brun, M. P., Bischoff, L., and Garbay, C. (2004) A very short route to enantiomerically pure coumarin-bearing fluorescent amino acids. *Angew. Chem., Int. Ed. 43*, 3432–3436.

(44) Lee, J. H., Choi, B. S., Chang, J. H., Lee, H. B., Yoon, J. Y., Lee, J., and Shin, H. (2007) The decarboxylative Blaise reaction. *J. Org. Chem. 72*, 10261–10263.

(45) Tararov, V. I., Korostylev, A., Konig, G., and Borner, A. (2006) Facile preparation and purification of mono tert-butyl malonate. *Synth. Commun. 36*, 187–191.

(46) Brooks, D. W., Lu, L. D. L., and Masamune, S. (1979) C-Acylation Under Virtually Neutral Conditions. *Angew. Chem., Int. Ed. Engl. 18*, 72–74.

(47) Sui, G., Mabrouki, M., Ma, Y., Micic, M., and Leblanc, R. M. (2002) A structural study of amphiphilic PAMAM (poly(amido amine)) dendrimers in Langmuir and Langmuir-Blodgett films. *J. Colloid Interface Sci. 250*, 364–370.

(48) Young, T. S., Ahmad, I., Yin, J. A., and Schultz, P. G. (2010) An enhanced system for unnatural amino acid mutagenesis in E. coli. *J. Mol. Biol. 395*, 361–374.

(49) Yao, X. L., and Hong, M. (2006) Effects of anionic lipid and ion concentrations on the topology and segmental mobility of colicin Ia channel domain from solid-state NMR. *Biochemistry 45*, 289–295.

(50) Lambotte, S., Jasperse, P., and Bechinger, B. (1998) Orientational distribution of alpha-helices in the colicin B and E1 channel domains: a one and two dimensional 15N solid-state NMR investigation in uniaxially aligned phospholipid bilayers. *Biochemistry 37*, 16–22.

(51) Schendel, S. L., and Reed, J. C. (2000) Measuring pore formation by Bcl-2 family proteins. *Methods Enzymol. 322*, 274–282.

(52) Huster, D., Xiao, L., and Hong, M. (2001) Solid-state NMR investigation of the dynamics of the soluble and membrane-bound colicin Ia channel-forming domain. *Biochemistry 40*, 7662–7674.

(53) Prieto, L., and Lazaridis, T. (2011) Computational studies of colicin insertion into membranes: the closed state. *Proteins 79*, 126–141.